

Microstructural evolution and mechanical strengthening mechanism of Mg-3Sn-1Mn-1La alloy after heat treatments

Zhanyong Zhao^a, Peikang Bai^{a,*}, Renguo Guan^c, Vignesh Murugadoss^{b,d}, Hu Liu^{b,e},
Xiaoqing Wang^{b,f}, Zhanhu Guo^{b,*}

^a School of Materials Science and Engineering, North University of China, Taiyuan 030051, China

^b Integrated Composites Laboratory, Department of Chemical and Biomolecular Engineering, University of Tennessee, Knoxville, TN 37996, USA

^c School of Materials Science and Engineering, Northwestern Polytechnical University, Xi'an 710072, China

^d Electrochemical Energy Research Lab, Centre for Nanoscience and Technology, Pondicherry University, Puducherry 605014, India

^e National Engineering Research Center for Advanced Polymer Processing Technology, Zhengzhou University, Zhengzhou 450002, China

^f School of Material Science and Engineering, Jiangsu University of Science and Technology, Zhenjiang, Jiangsu 212003, China

ARTICLE INFO

Keywords:

Mg alloy
Precipitation
Heat treatments
Microstructure
Mechanical Properties

ABSTRACT

The Mg-3Sn-1Mn-1La alloy sheets were prepared by a continuous reo-rolling process, and the effects of the solution and aging treatment on the microstructures and mechanical properties of the alloy were studied. The tensile strength and elongation at room temperature and 150 °C of the Mg-3Sn-1Mn-1La alloy sheets were decreased with increasing the solution time. The grain size was increased gradually. The plate-shaped MgSnLa compounds composed of La₅Sn₃, Mg₂Sn and Mg₁₇La₂ phases and Mg₂Sn phase gradually disappeared. At the same time, new irregular MgSnLa compounds were formed in grains. Aging treatment of the alloy was performed after solution treatment. The new spherical MgSnLa compounds composed of La₅Sn₃, Mg₂Sn and Mg₁₇La₂ phase were formed, increased and distributed gradually homogeneously in the matrix with increasing the aging treatment time. Meanwhile, the Mg₂Sn phases with spherical, short-rod and lath-shaped were formed in the matrix. After solution treatment at 550 °C for 24 h, aging at 250 °C for 48 h, the tensile strength at room temperature and at 150 °C of the Mg-3Sn-1Mn-1La alloy sheet was increased to 270 MPa and 233 MPa, with 19% and 20% increase, respectively. The elongation at room temperature and 150 °C was increased to 7.9% and 67.5%, with 6% and 4% increase, respectively. The formed spherical MgSnLa compounds and Mg₂Sn phases which were coherent with the matrix and effectively pinned the dislocations and grain boundaries were responsible for the enhanced mechanical properties of the alloys.

1. Introduction

Magnesium(Mg) alloys have been widely applied in aerospace, military, transportation, and 3C (computers, communication, and consumed electronics) products because of their high specific strength and stiffness, shock absorbing capacity, good casting performance, strong electromagnetic shielding ability and so on [1,2]. However, it is difficult to process at low temperature due to the hexagonal close-packed (HCP) lattice structure and less slip system. In addition, poor heat resistance of Mg alloys and lower melting temperature of Mg₁₇Al₁₂ phase (498 °C) in commercial AZ series and AM series Mg alloys hinder the use of Mg alloys in various applications [3].

The main way to improve the strength and heat resistance of magnesium alloy is to form micro-alloying, which promotes the

precipitation of the strengthening phase. The strengthening phase could pin the dislocations and grain boundaries and improve the mechanical properties of Mg alloy. The addition of Si and Sn elements into the Mg alloys makes the Mg₂Si or Mg₂Sn phases thermally stable and possess high hardness, which improves the mechanical properties of Mg alloys at room and high temperatures [4]. The melting temperature of Mg₂Sn phase (778 °C) is higher than that of Mg₁₇Al₁₂ phase (498 °C), and the hardness of the Mg₂Sn phase is higher (119 HV), thus the Mg₂Sn phase with high melting temperature and high hardness enhances the mechanical properties and thermal stability [5–7]. Yang et al. reported that Mg-3Sn-2Ca alloy exhibits higher creep properties at 150 °C [8]. Zhao et al. found that the Sn content significantly improved the tensile strength, yield strength, and the elongation of Mg-Sn alloy [9]. Rare earth (RE) elements have been added to Mg-Sn alloys to further

* Corresponding authors.

E-mail addresses: baipeikang@nuc.edu.cn (P. Bai), zguo10@utk.edu (Z. Guo).

<https://doi.org/10.1016/j.msea.2018.07.083>

Received 3 June 2018; Received in revised form 22 July 2018; Accepted 23 July 2018

Available online 29 July 2018

0921-5093/ © 2018 Elsevier B.V. All rights reserved.

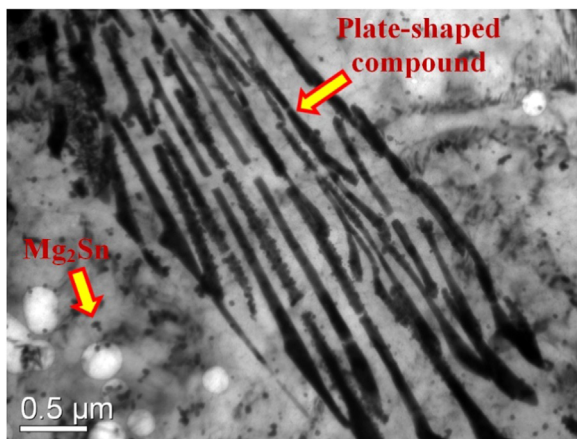


Fig. 1. MgSnLa plate-shaped compounds composed of La_5Sn_3 , Mg_2Sn and $\text{Mg}_{17}\text{La}_2$ phases and Mg_2Sn phases in the Mg-3Sn-1Mn-1La alloy sheet prepared by the rheo-rolling process.

enhance their mechanical properties. Wei et al. found that the La element significantly increased the high temperature strength of Mg-5Sn alloy due to the formed rare-earth strengthening phase in the Mg-xSn-2La alloy [10]. Liu et al. studied the effect of didymium(Di) and strontium(Sr) on the microstructure and properties of Mg-5%Sn alloy and found that the Sn-Di phase improved the creep resistance of Mg-5%

Sn-2%Di alloy [11]. Pan et al. found that adding 0.43 wt% Zr, 0.87 wt% Ce and 0.36 wt% Sc elements could improve the mechanical properties of Mg-3Sn-1Mn alloy [12]. Recently, we prepared the Mg-3Sn-1Mn-1La alloy sheet by the continuous rheo-rolling process whose tensile strength and elongation were 230 MPa and 7.5% respectively, which were 29% and 32% higher than that of the Mg-3Sn-1Mn alloy sheet without La element, respectively [13].

According to previous investigations, heat treatment is one of the effective methods for improving the mechanical properties of the Mg-Sn alloy [14–16]. For example, Nayyeri et al. reported the enhanced creep resistance of the material in the aged condition which was related to the dispersive distribution of Mg_2Sn phase in the Mg matrix [17]. Elsayed et al. revealed that the hardness of Mg-9.8Sn-3.0Al-1.0Zn-0.1Na reached a peak value of 100 HV by effective aging hardening [18]. Sasaki et al. reported that Mg-5.4Sn-4.2Zn-2.0Al-0.2Mn-0.1Na alloy exhibited a significant increase in the yield strength from 243 to 347 MPa after T6 treatment [19]. Wei et al. demonstrated that the compressive creep resistance of the aged Mg-5Sn alloy was much better than that of the as-cast material [20]. Kim et al. reported a uniform distribution of Mg_2Sn and I-phase particles formed inside the alloy after homogenization treatment, which enhanced the strength of Mg-Sn-Al alloy [21].

The research results show that the heat treatment strengthening of Mg-Sn alloy is mainly due to the precipitation strengthening of the Mg_2Sn phase [22–24]. However, the heat treatment of Mg-Sn alloy containing rare earth elements was less studied. The Mg-3Sn-1Mn-1La alloy sheet was prepared by a continuous rheo-rolling process. The plate-shaped MgSnLa compounds composed of La_5Sn_3 , Mg_2Sn and

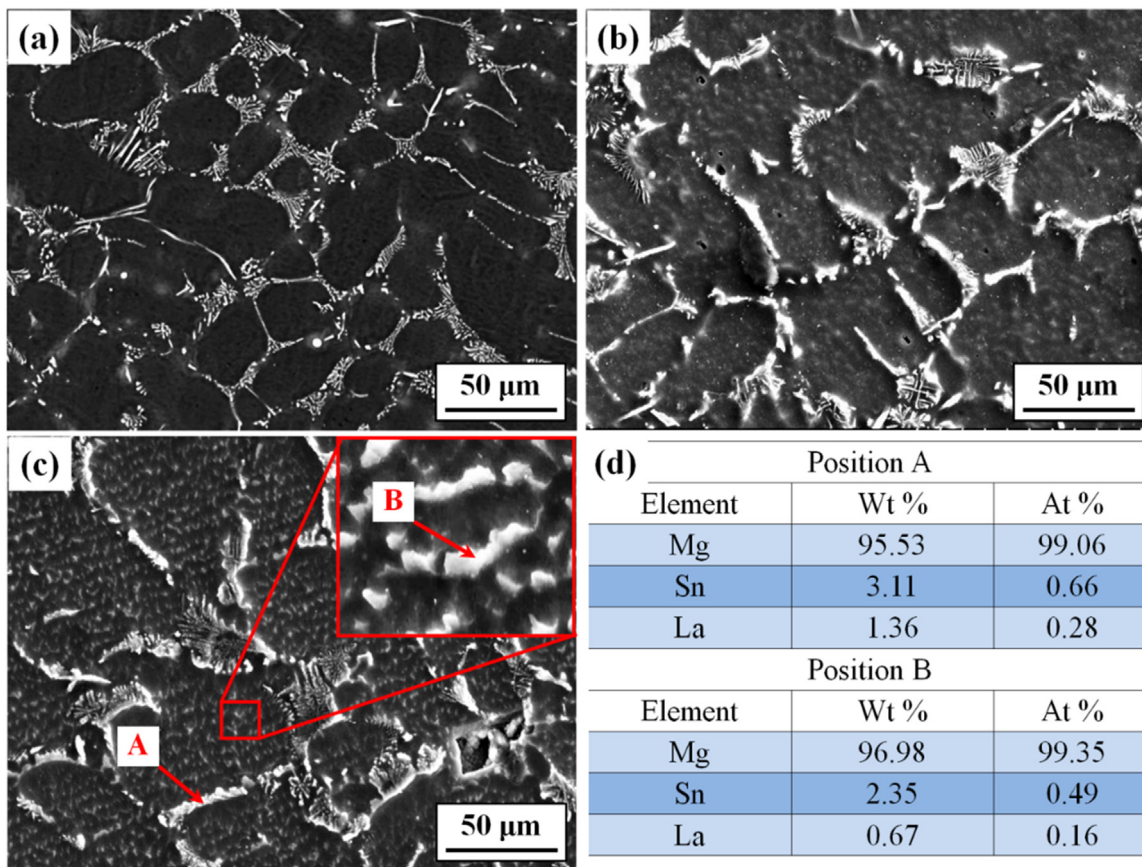


Fig. 2. SEM micrographs of (a) Mg-3Sn-1Mn-1La alloy before solution treatment; (b) solution at 550 °C for 8 h; (c) solution at 550 °C for 24 h; and (d) composition analysis at point A and B.

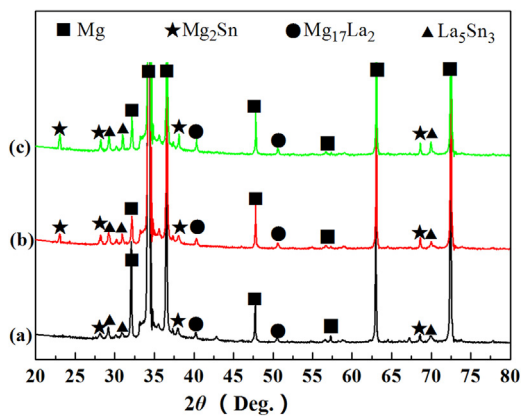


Fig. 3. XRD patterns for the Mg-3Sn-1Mn-1La alloys after different heat treatments: (a) solution at 550 °C for 24 h, (b) solution at 550 °C for 24 h, aging at 250 °C for 0.03 h, (c) solution at 550 °C for 24 h, aging at 250 °C for 48 h.

$Mg_{17}La_2$ phases and Mg_2Sn phases were formed and improved the mechanical properties of the alloys [13]. However, little work has been done on the heat treatment behaviors of Mg-3Sn-1Mn-1La alloys either.

In this study, the effects of the solution and aging heat treatment on the microstructure and properties of Mg-3Sn-1Mn-1La alloy sheet produced by the rheo-rolling process were studied. The objective of the study described here is to reveal phase transformation occurring during the heating process, and to elucidate the effect of the phase on the mechanical properties of Mg-3Sn-1Mn-1La alloy.

2. Experimental procedure

Mg-3Sn-1Mn-1La alloy sheet was prepared by the continuous rheo-rolling, as previously described in details [13,25]. Briefly, a molten alloy was cast onto the vibrating slope plate to form a high-quality semi-solid metal slurry via flow shear and vibration effects. This semi-solid metal slurry entered directly into the bottom of the width-restricted roll for rheo-rolling. The Mg-3Sn-1Mn-1La alloy sheet was solution treated at 550 °C for 2–30 h, and then the samples were quenched in water. The samples were aged at 250 °C for 0–144 h after the solution treatment.

The specimens (15 mm × 15 mm × 10 mm) were cut from the Mg-3Sn-1Mn-1La after different heat treatments, the phase identification of the surface was performed in an X-ray diffraction (XRD) (X'Pert, PANalytical B.V., Almelo, Holland). The specimens were polished and etched with a solution of 15 mL HCl + 56 mL C_2H_5OH + 47 mL H_2O . The microstructure and distribution of elements of samples were examined by scanning electron microscope (SEM) (Zeiss Ultra 55, Carl Zeiss Microscopy, Jena, Germany) equipped with energy dispersive spectroscopy (EDS). The sample was processed into a $\Phi 3 \times 0.5$ mm discs using a spark-cutting machine (DK7740, Precision Machinery Co., Ltd, China), the discs were ground to a thickness of 80 μm and further thinned using a precision ion polishing system (Gatan 691, USA). The TEM observations were performed using field-emission-gun (FEG) Tecnai G² 20 microscope (FEI, Oregon, USA) operating at an accelerating voltage of 200 kV. The age hardening behavior was measured by a Vickers hardness tester (TMHVS-1000, Shanghai Tuming Optical Instrument CO., LTD) under a load of 2000 g and a holding time of 25 s. The mechanical properties of the Mg-3Sn-1Mn-1La sheets were

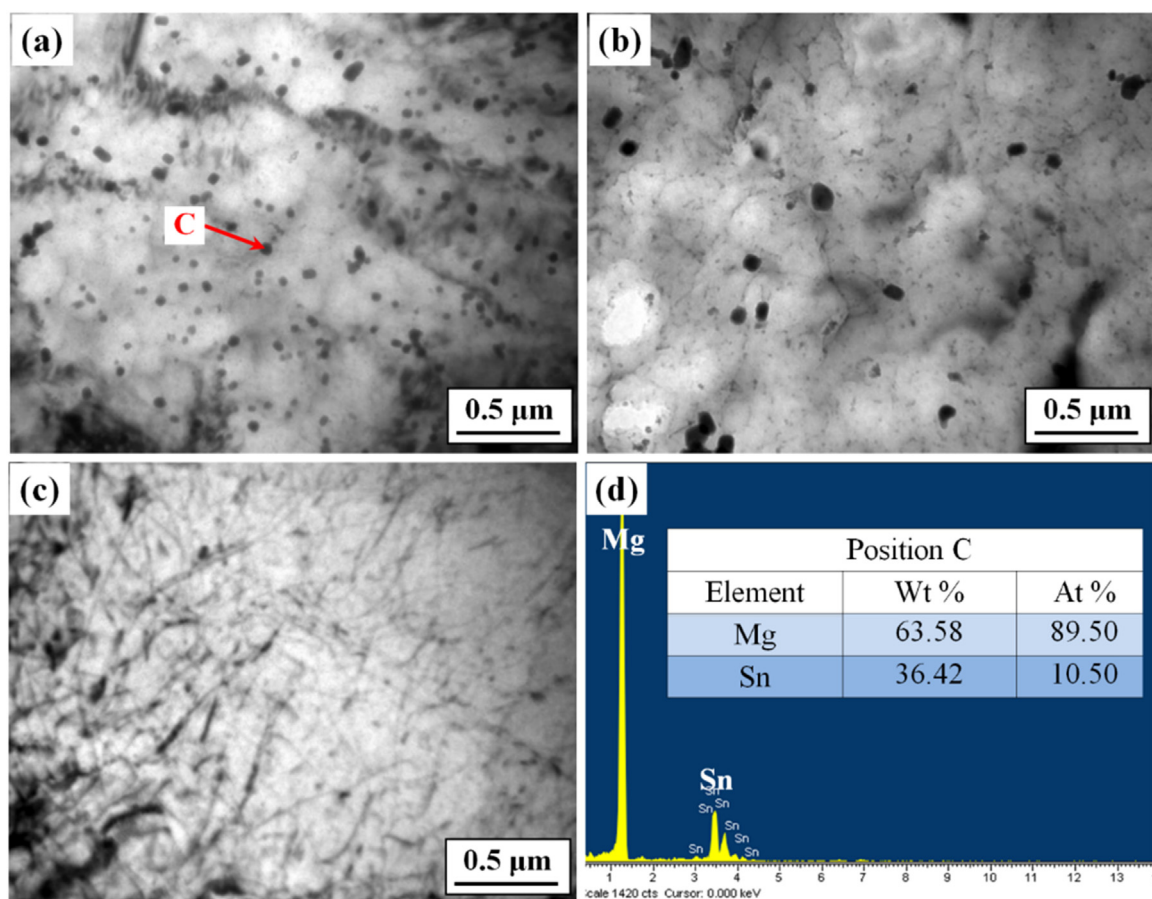


Fig. 4. TEM microstructures of Mg-3Sn-1Mn-1La observed along $[0001]_{Mg}$ zonal axis: (a) Mg-3Sn-1Mn-1La alloy before solution treatment, (b) solution at 550 °C for 24 h, (c) solution at 550 °C for 24 h, (d) composition analysis at point C.

evaluated on MTS 810 mechanical properties testing system (MTS, USA). The strain rate was $5 \times 10^{-3} \text{ s}^{-1}$ at room temperature and 150 °C. A MTS LX300 laser extensometer was used to calibrate and measure the strain of the sample on the tensile loading.

3. Results

3.1. Precipitation behaviors and mechanical properties during solution treatments

Previous research has shown that a MgSnLa plate-shaped compound composed of La_5Sn_3 , Mg_2Sn and $\text{Mg}_{17}\text{La}_2$ phases and Mg_2Sn was formed in the Mg-3Sn-1Mn-1La sheet prepared by the rheo-rolling process [13], as shown in Fig. 1. The plate-shaped compound pinned the α -Mg grain boundaries and dislocations. The Mg-3Sn-1Mn-1La (wt%) alloy plate exhibited a tensile strength of 230 MPa and elongation of 7.5% [13].

Fig. 2 shows the SEM micrographs of the Mg-3Sn-1Mn-1La alloy sheets which were prepared by rheo-rolling process and were solution treated at 550 °C for different time intervals. The grain size of the alloy was gradually increased with increasing the solution time. However, the plate-shaped MgSnLa compounds at the grain boundary and the Mg_2Sn phase in the grains gradually decreased. At the same time, new irregular phase was formed in the grains.

Based on EDS and XRD (Figs. 2d and 3, respectively), the compounds formed in the grains were determined to be MgSnLa compounds composed of La_5Sn_3 , Mg_2Sn and $\text{Mg}_{17}\text{La}_2$ phases. When the Mg-3Sn-1Mn-1La was solution treated at 550 °C for 24 h, the spherical Mg_2Sn phase in the grains completely was dissolved into the α -Mg matrix (Fig. 4), irregular MgSnLa compounds (Fig. 2c, points A and B) were formed.

Fig. 5a and b shows the engineering stress-strain curves of Mg-3Sn-1Mn-1La alloy tested at room temperature and 150 °C after solution treatment. With the increase of solution treatment time, the tensile strength and elongation of Mg-3Sn-1Mn-1La alloy were decreased both at room temperature and 150 °C (Fig. 5c). When the alloy was solution treated at 550 °C for 24 h, the tensile strength and elongation of the Mg-3Sn-1Mn-1La alloy at room temperature were decreased from 230 MPa 7.5% to 185 MPa, and 5.5% respectively. The tensile strength and elongation at 150 °C were decreased from 194 MPa, 65% to 161 MPa, 48%.

3.2. Precipitation behaviors and mechanical properties during aging treatment

After solution treatment at 550 °C for 24 h, the Mg-3Sn-1Mn-1La alloys were aged at 250 °C for different time intervals. Fig. 6 shows the effect of aging time on the hardness of Mg-3Sn-1Mn-1La alloy. With the increase of aging time, the hardness of samples was increased. When the aging time was increased to 48 h, the hardness of alloy reached peak (53 HV). Then the hardness of alloy was decreased with increasing the aging time.

Fig. 7 shows the SEM micrographs and EDS analysis of Mg-3Sn-1Mn-1La alloy with different aging time intervals. With increasing the aging time, the precipitation phases which mainly contained Mg, Sn and La gradually were formed and increased at grain boundaries. The EDS (Fig. 7d) and XRD results (Fig. 3) suggested that the precipitation phases at grain boundaries were MgSnLa compound phase composed of La_5Sn_3 , Mg_2Sn and $\text{Mg}_{17}\text{La}_2$. The irregular MgSnLa compounds which were formed during the solution in the grains gradually disappeared.

At the beginning of aging treatment (0.03 h), spherical phases with different sizes were formed at the grain boundary (Fig. 8a). The larger spherical phase (average diameter ≥ 70 nm) contained the element Mg, Sn and La, while the smaller spherical phase (average diameter \leq

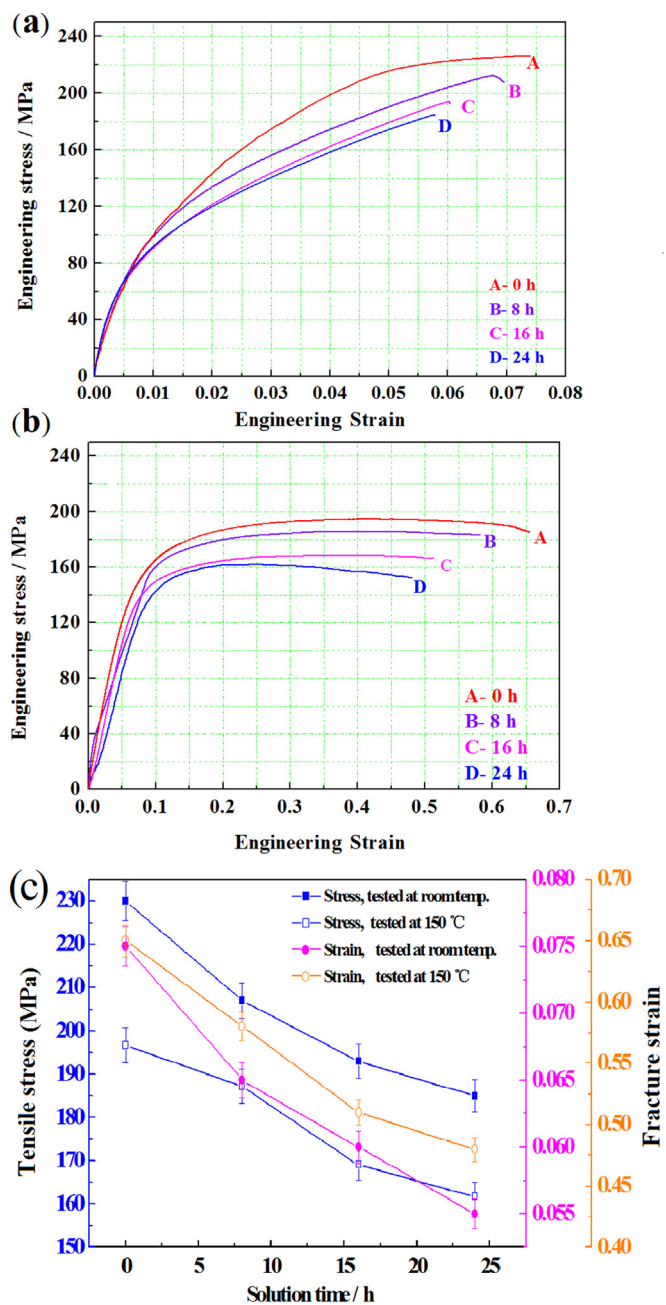


Fig. 5. Engineering stress-strain curves for Mg-3Sn-1Mn-1La alloy sheets with solution treated at 550 °C. (a) at room temperature, (b) at 150 °C, (c) Evolution of tensile stress and strain at different temperatures with different solution treatments.

40 nm) mainly contained the element Mg and Sn (Fig. 8d). According to the results of XRD pattern (Fig. 3), it can be inferred that the spherical phase with larger size (average diameter ≥ 70 nm) was MgSnLa compound, the spherical phase with smaller size (average diameter ≤ 40 nm) was Mg_2Sn phase, and the plate-shaped MgSnLa compound formed during the rheo-rolling process was not observed (Fig. 8). With increasing the aging time, the spherical MgSnLa compounds were gradually increased. When the aging time reached 48 h, the average diameter of the spherical MgSnLa compound increased to 170 nm, and

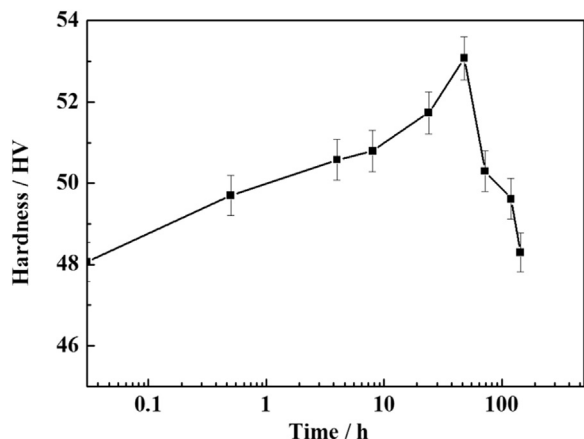


Fig. 6. Age-hardening curves during artificial aging at 250 °C for different time intervals (load: 2000 g).

were distributed homogeneously (Fig. 8b). When the aging time was more than 48 h, over aging was initiated, the spherical MgSnLa compounds further grew and agglomerated severely (Fig. 8c).

At the beginning of aging, the spherical Mg₂Sn phase was formed at the grain boundary and in grains, the particle size of Mg₂Sn phase was about 40 nm. When the aging time increased to 48 h, the spherical Mg₂Sn phase increased to an average diameter of 50 nm, meanwhile, the Mg₂Sn phase with short-rod and lath-shaped was formed in the matrix, as shown in Fig. 9.

Fig. 10 shows the engineering stress-strain curves of Mg-3Sn-1Mn-1La alloy after solution treatment at 550 °C for 24 h and aging at 250 °C

for different time intervals. As the aging time increased, the tensile strength and elongation of Mg-3Sn-1Mn-1La alloy at room temperature and 150 °C were increased gradually (Fig. 10d). After solution treatment at 550 °C for 24 h, aging at 250 °C for 48 h, the tensile strength at room temperature and at 150 °C of Mg-3Sn-1Mn-1La alloy sheet was increased to 270 and 233 MPa, with 19% and 20% increase. The elongation at room temperature and 150 °C was increased to 7.9% and 67.5%, with 6% and 4% increase, respectively, as shown in Fig. 10a and b.

4. Discussion

4.1. Effect of solution treatment on mechanical properties

The tensile strength of the Mg-3Sn-1Mn-1La alloy at room temperature and high temperature gradually was decreased with increasing the solution treatment time (Fig. 5). This was because the Mg-3Sn-1Mn-1La alloy sheet prepared by rheo-rolling contained Mg₂Sn phases and plate-shaped MgSnLa compounds. The Mg₂Sn phases and plate-shaped MgSnLa compounds were coherent with the α-Mg matrix and effectively pinned the dislocations and grain boundary, which could enhance the mechanical properties of the alloy [13]. However, during the solution treatment, the Mg₂Sn phases and plate-shaped MgSnLa compounds were gradually dissolved into the matrix (Fig. 4), and the strengthening effect of Mg₂Sn phases and plate-shaped MgSnLa compounds gradually decreased.

Although new irregular MgSnLa compound was formed in the grains, the irregular MgSnLa compounds were distributed inhomogeneously (Fig. 11a) and were incoherent with the α-Mg matrix. There was lattice distortion near the bonding interface between the α-Mg matrix and the irregular MgSnLa compound (Fig. 11b). The strengthening effect of the new irregular MgSnLa compound was lower

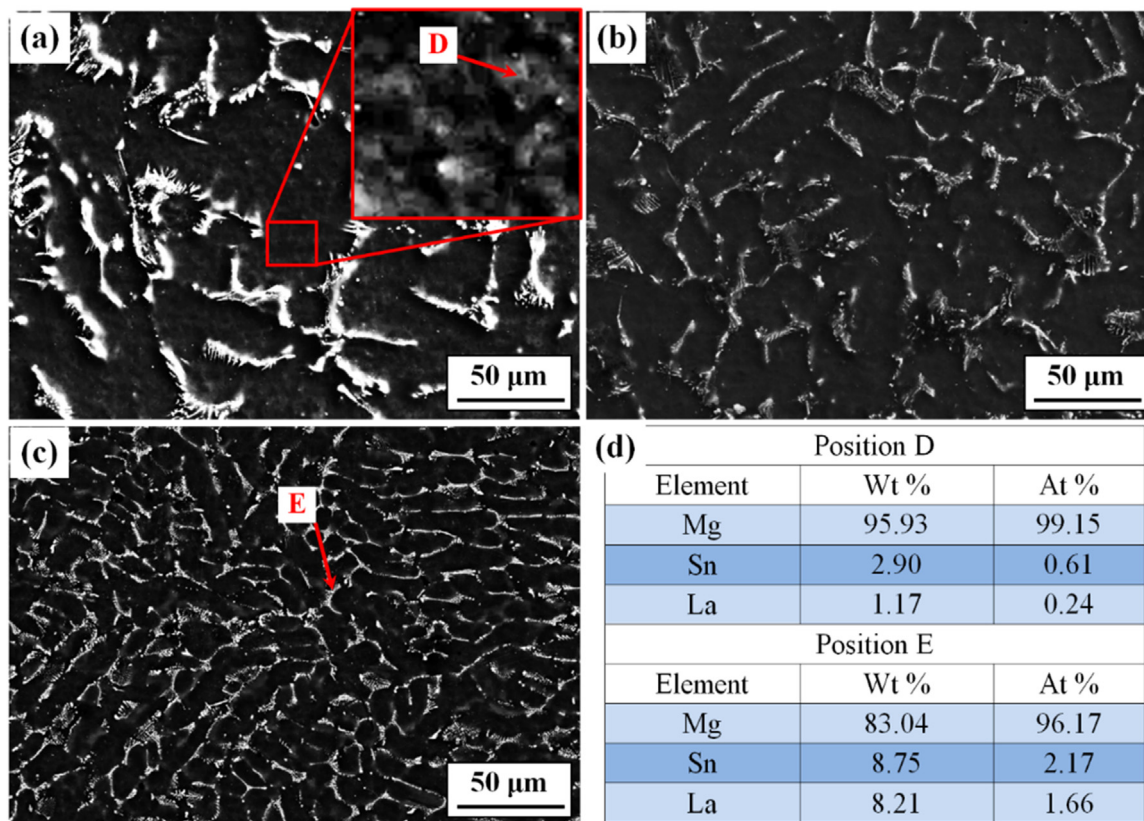


Fig. 7. SEM microstructures of Mg-3Sn-1Mn-1La alloy (a) solution at 550 °C for 24 h aging at 250 °C for 0.03 h, (b) solution at 550 °C for 24 h aging at 250 °C for 48 h, (c) solution at 550 °C for 24 h, aging at 250 °C for 56 h, (d) composition analysis at point D and E.

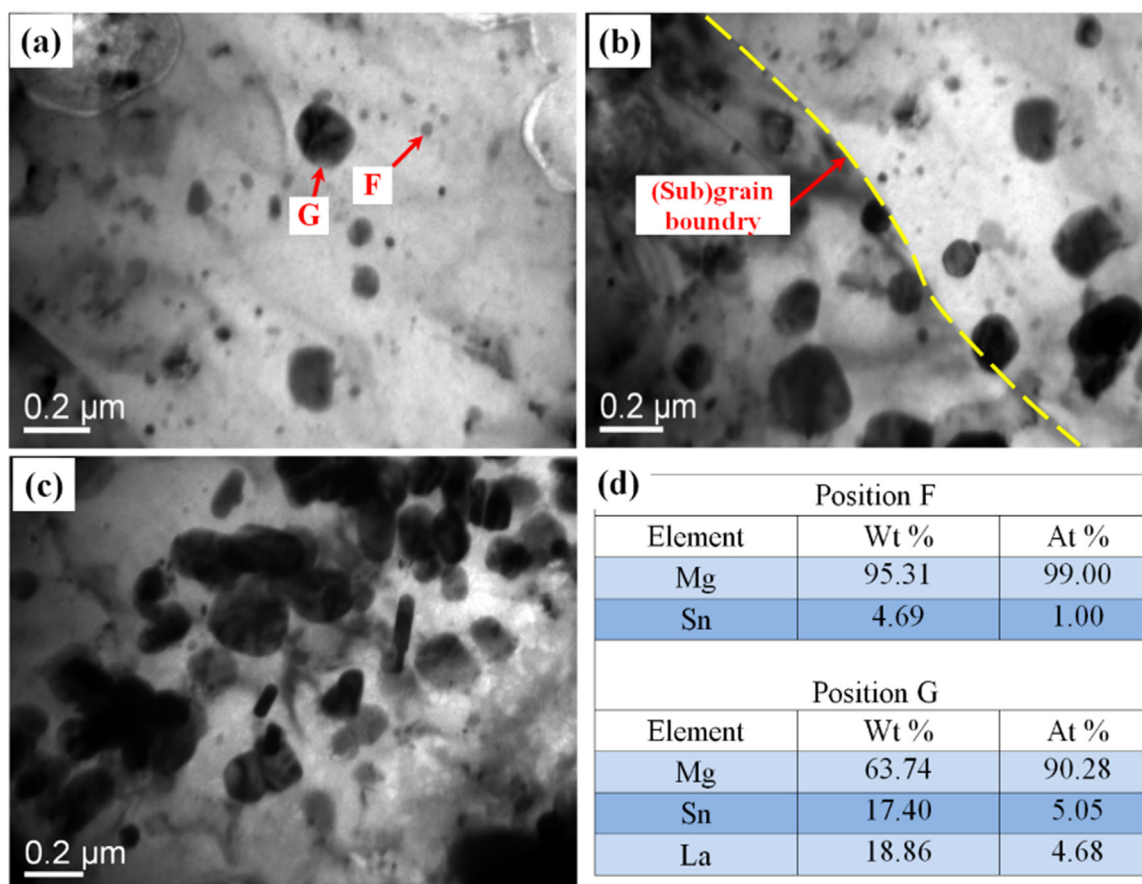


Fig. 8. TEM microstructures of Mg-3Sn-1Mn-1La alloy (a) solution at 550 °C for 24 h aging at 250 °C for 0.03 h, (b) solution at 550 °C for 24 h, aging at 250 °C for 48 h, (c) solution at 550 °C for 24 h aging at 250 °C for 56 h, (d) composition analysis at point F and G.

than that of the combined action of Mg_2Sn phases and plate-shaped $MgSnLa$ compounds, so the tensile strength of the Mg-3Sn-1Mn-1La alloy at room temperature and high temperature gradually was decreased during the solution treatment.

The new irregular $MgSnLa$ compounds were formed in the grains during the solution treatment, because the solid solubility of La in the α -Mg matrix was 0.74% [26,27]. The content of La element in the alloy is 1%, and the La cannot be completely dissolved in the α -Mg matrix during the solution treatment, some La exist in the form of precipitated phase. Before solution treatment, the plate-shaped $MgSnLa$ compounds were mainly distributed at the grain boundary [13], the La concentration at grain boundaries was high. When solution treatment began, the plate-shaped $MgSnLa$ compounds were gradually dissolved into the matrix. At the same time, the La moved from the high concentration region of grain boundary to the low concentration of grains and was homogeneously distributed within the matrix. However, some La existed in the form of new irregular $MgSnLa$ compounds, as the content of La element exceeded the solid solubility limit. At the same time, because of the high solution temperature, the new irregular $MgSnLa$ compounds were unstable, and dissolved into the matrix, which were in dynamic equilibrium. The interfacial energy between irregular $MgSnLa$ compounds and the matrix was relatively high, and the interfacial atom arrangement was disordered. When the Mg-3Sn-1Mn-1La alloys were solution treated at 550 °C for 24 h and quenched in water, new irregular $MgSnLa$ compounds were formed, and were incoherent with α -Mg matrix, as shown in Fig. 11b.

4.2. Effect of aging treatment on mechanical properties

After aging treatment, the fine spherical Mg_2Sn phase was formed in the grains (Fig. 8), and they were coherent with α -Mg matrix (Fig. 12a). The spherical Mg_2Sn phase and α -Mg matrix have a small degree of mismatch (Fig. 12a) and low interfacial strain, and their interface is relatively stable, which pin the dislocation and grain boundary, inhibit the microcracks, coordinate lattice distortion during deformation, and enhance the mechanical properties of the alloy [28]. There were the short-rod and lath-shaped Mg_2Sn phase in the matrix, as shown in Fig. 9a, b and c. The diffraction patterns of α -Mg matrix were shown in Fig. 9d, these spots were indexed as α -Mg phase (HCP, $A = 0.32080$, $B = 0.32080$, $C = 0.52090$) according to the $[0001]_{\alpha}$ zone axis. Fig. 9e shows the diffraction pattern of the short-rod Mg_2Sn , the spots indicated $R21 = 2.539$, $R22 = 2.99$, along with an angle of 53.7° between $R21$ and $R22$. Therefore, these spots were indexed as Mg_2Sn phase (FCC, $A = 0.67590$, $B = 0.67590$, $C = 0.67590$) according to the $[110]_{Mg_2Sn}$ zone axis. The orientation relationships of the short-rod Mg_2Sn phase and α -Mg matrix were as follows: lattice plane $(-211)_{Mg_2Sn} // (-1010)_{Mg}$, axis $\langle 011 \rangle_{Mg_2Sn} // \langle 0001 \rangle_{Mg}$. Fig. 9f shows the diffraction pattern of lath-shaped Mg_2Sn , the spots indicated $R11 = 4.1$, $R12 = 4.2$, along with an angle of 60° between $R11$ and $R12$. Therefore, these spots were indexed as Mg_2Sn phase (FCC, $A = 0.67590$, $B = 0.67590$, $C = 0.67590$) according to the $[111]_{Mg_2Sn}$ zone axis. The orientation relationships of the lath-shaped Mg_2Sn phase and α -Mg matrix were as follows: lattice plane lattice plane $(-1\ 1\ 1)_{Mg_2Sn} // (-1010)_{Mg}$, $\langle 111 \rangle_{Mg_2Sn} // \langle 0001 \rangle_{Mg}$. Huang and Shi et al. found

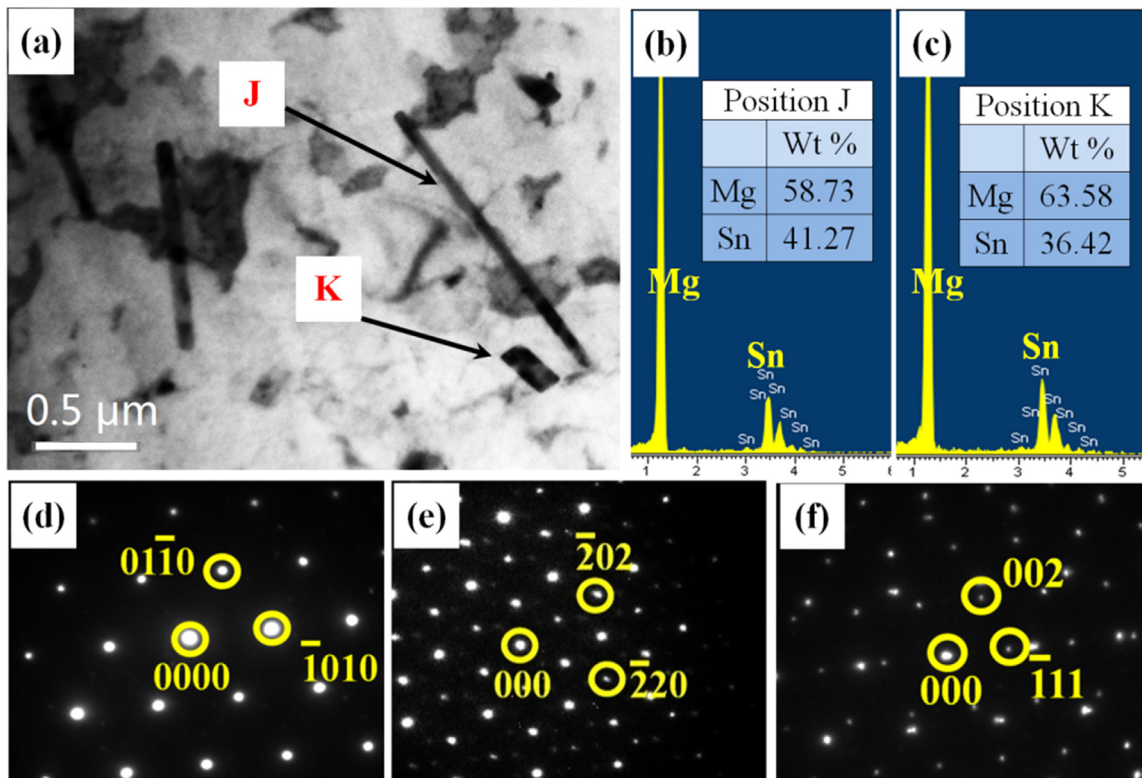


Fig. 9. TEM microstructures of Mg-3Sn-1Mn-1La alloy with solution treatment at 550 °C for 24 h aging at 250 °C for 48 h (a), EDS analysis of the precipitate (b, c), superimposed diffraction patterns of the matrix (d) and the precipitate (e, f).

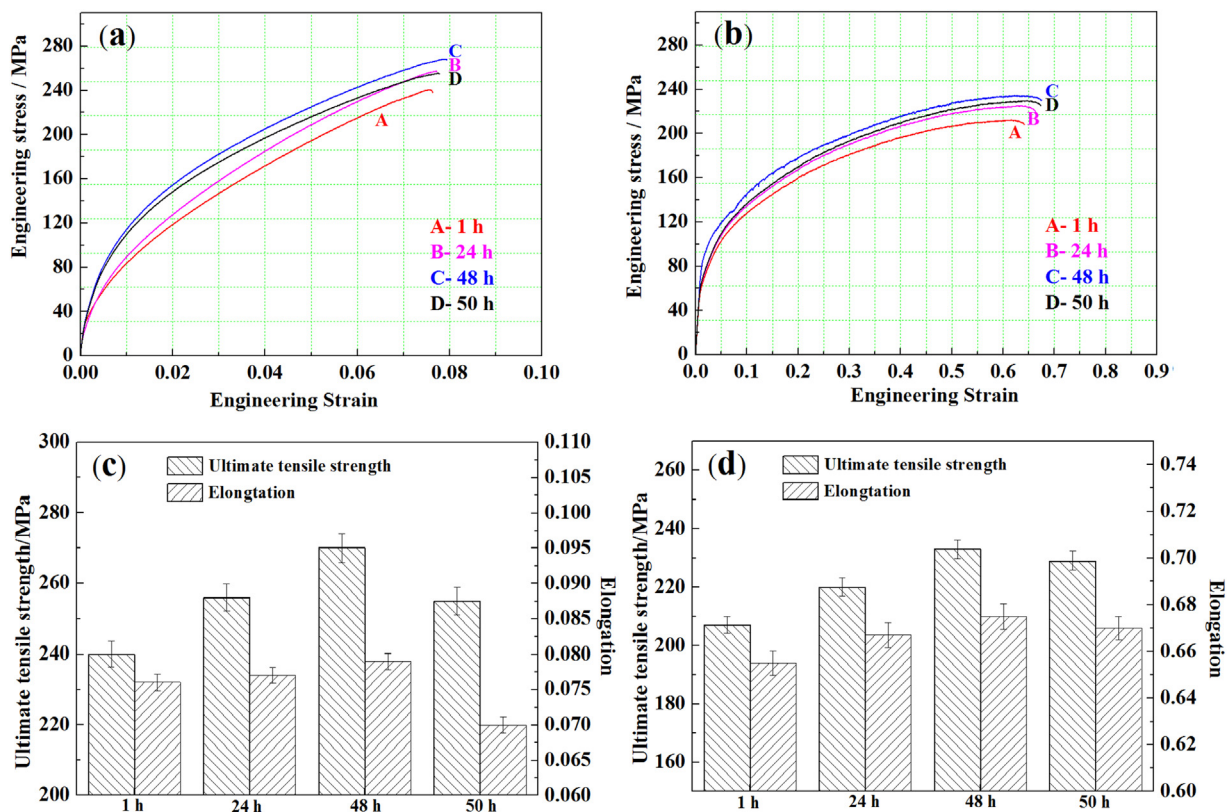


Fig. 10. Engineering stress-strain curves for Mg-3Sn-1Mn-1La alloy sheets aging at 250 °C for different time intervals. (a) at room temperature, (b) at 150 °C, the comparison of the tensile stress and strain aging at 250 °C for different time intervals. (c) at room temperature, (d) at 150 °C.

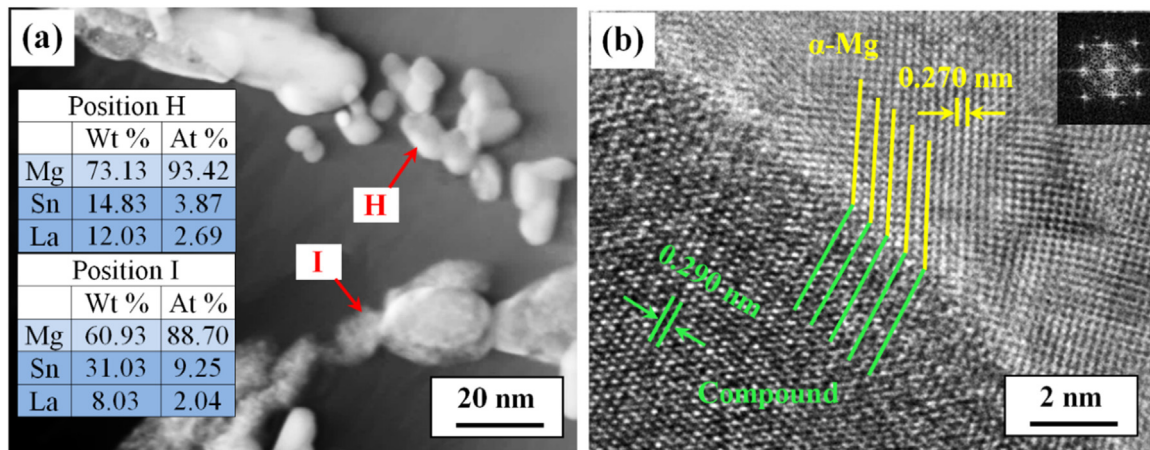


Fig. 11. TEM images (a) of Mg-3Sn-1Mn-1La solution at 550 °C for 24 h, High-resolution TEM images (b) of the MgSnLa compound and α -Mg, inset of (a) shows the elemental analysis at position of H and I.

the new relationship between the Mg_2Sn phase and the α -Mg matrix in the Mg alloy [29,30]. The Mg_2Sn phase with spherical, short-rod and lath-shaped has a coherent relationship with the matrix, and effectively pins the dislocation movement during the deformation process at room temperature and high temperature, thus improves the mechanical properties of the alloy. Zhang et al. also reported that Mg-4.5Zn-4.5Sn-2Al alloy formed lath-shaped Mg_2Sn phase after solid solution aging treatment, which effectively improved the mechanical properties of the alloy [31].

During aging treatment, the spherical MgSnLa compounds composed of La_5Sn_3 , Mg_2Sn and $Mg_{17}La_2$ phase were formed firstly. Most of the precipitates easily nucleated at the grain boundaries and defects, especially at the large-angle grain boundaries. That was because the lattice mismatch of the interface was larger, energy was relatively high, and the defects at the interface were also more than in grains, which could improve the diffusion of the element and the nucleation and growth of the precipitated phase. At the beginning of aging, the electronegativity difference between La and Sn was larger (0.86), La_5Sn_3 phase first nucleated at the grain boundary [13]. After La_5Sn_3 nucleated, there were enough La atoms and Sn atoms to promote the nucleation growth. The electronegativity difference between Mg and Sn (0.65) was greater than that between Mg and La (0.21), thus, the Mg_2Sn phase nucleated on the La_5Sn_3 phase, then the $Mg_{17}La_2$ phase finally nucleated on the Mg_2Sn phase [13]. Therefore, the La_5Sn_3 , Mg_2Sn and $Mg_{17}La_2$ phases nucleated and grew alternately, forming a spherical MgSnLa compound comprising of three phases.

During the aging treatment, Mg, Sn and La elements were uniformly distributed around the nucleation of the spherical MgSnLa compounds, there was no external interference, the Mg, Sn, and La elements uniformly moved. The precipitation of MgSnLa compounds was a Gibbs decreasing process. The system always proceeded spontaneously toward the direction of energy reduction. However, due to the formation of a solid secondary phase, the surface energy increased. If the process proceeds, the surface energy must be reduced. The surface area of the sphere was the smallest when the volume features were the same, so the MgSnLa compounds approached to sphericity. With increasing the aging time, the spherical MgSnLa compounds grew up, the La and Sn atoms near the grain boundary gradually decreases, the La atoms and Sn atoms need to diffuse from the grains. Therefore, the spherical MgSnLa compounds grew perpendicular to the boundary and toward the inside of the α -Mg matrix, which pinned the grain boundaries, and impeded the boundary sliding (Fig. 8b), improved the stability of alloy at high temperature. When the aging time reached 48 h, the average

diameter of the spherical MgSnLa compounds increased to 170 nm, and were distributed homogeneously (Fig. 8b).

During the deformation of Mg-3Sn-1Mn-1La alloy, the spherical MgSnLa compounds effectively pinned the dislocations, a large number of dislocations moved and aggregated near the MgSnLa compounds (Fig. 12c), resulting in large lattice distortion and the stacking or micro twins formation (Fig. 12b). The spherical MgSnLa compounds effectively accommodated the movement of dislocations and micro twins. The coordination of the stacking faults and the micro twins was improved, which enhanced the mechanical properties of the alloy. When the aging time was more than 48 h, overaging occurred, the spherical MgSnLa compound phase further grew and agglomerated severely, the strengthening effect of the precipitation phase decreased, so the hardness and mechanical properties of the alloy were reduced (Figs. 6 and 10).

5. Conclusions

The effects of the solution and aging treatment on the microstructure and mechanical properties were studied in the Mg-3Sn-1Mn-1La alloy sheets prepared by the continuous rheo-rolling process. The tensile strength and elongation at room temperature and 150 °C of Mg-3Sn-1Mn-1La alloy sheet were decreased with increasing the solution time. The grain size increased gradually. The plate-shaped MgSnLa compounds composed of La_5Sn_3 , Mg_2Sn and $Mg_{17}La_2$ phases and Mg_2Sn phase gradually disappeared. At the same time, new irregular MgSnLa compounds were formed in grains. Aging treatment of the alloy was performed after solution treatment, the new spherical MgSnLa compounds composed of La_5Sn_3 , Mg_2Sn and $Mg_{17}La_2$ phase were formed, increased and distributed gradually homogeneously in the matrix with increasing the aging treatment time. Meanwhile, the Mg_2Sn phases with spherical, short-rod and lath-shaped were formed in the matrix. The spherical MgSnLa compounds and Mg_2Sn phases were coherent with the matrix, which effectively pinned the dislocations and grain boundaries to enhance the mechanical properties of the alloys. After solution treatment at 550 °C for 24 h, aging at 250 °C for 48 h, the tensile strength at room temperature and at 150 °C of Mg-3Sn-1Mn-1La alloy sheet was increased to 270 and 233 MPa, with 19% and 20% increase, respectively. The elongation at room temperature and 150 °C was increased to 7.9% and 67.5%, with 6% and 4% increase, respectively. Compared with polymer and carbon based systems with low thermal stability [32–59], the reported alloys here will have great high-temperature applications.

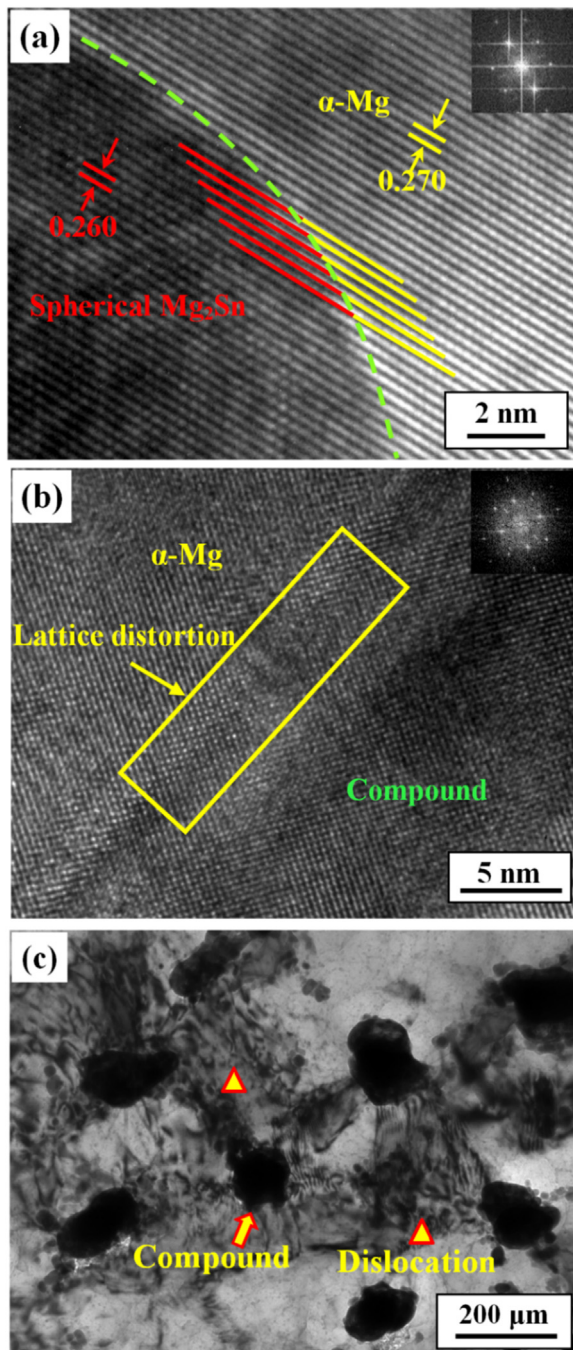


Fig. 12. High-resolution TEM images (a,b) of Mg_2Sn and $MgSnLa$ compound and (c) high density of dislocations impeded by the $MgSnLa$ compound (arrows).

Acknowledgements

This work was supported by the National Natural Science Foundation of China (Grant No. 51604246 and 51775521), the supports of the North University of China for Young Academic Leaders.

Conflict of interest

There are no conflicts of interest to declare.

References

- [1] A. Tehrani, B. Yin, W.A. Curtin, Solute strengthening of basal slip in Mg alloys, *Acta Mater.* 151 (2018) 56–66.
- [2] Z.Y. Zhao, R.G. Guan, J.H. Zhang, Z.Y. Zhao, P.K. Bai, Effects of process parameters of semisolid stirring on microstructure of Mg-3Sn-1Mn-3SiC (wt%) strip processed by Rheo-rolling, *Acta Metal. Sin. -Eng. Lett.* 30 (2017) 66–72.
- [3] Y. Tang, W. Goto, S. Hirotsawa, Z. Horita, S. Lee, K. Matsuda, D. Terada, Concurrent strengthening of ultrafine-grained age-hardenable Al-Mg alloy by means of high-pressure torsion and spinodal decomposition, *Acta Mater.* 131 (2017) 57–64.
- [4] J. Mao, H.S. Kim, J. Shuai, Z. Liu, R. He, U. Saramadu, F. Tian, W. Liu, Z. Ren, Thermoelectric properties of materials near the band crossing line in Mg_2Sn - Mg_2Ge - Mg_2Si system, *Acta Mater.* 103 (2016) 633–642.
- [5] H. Liu, Y. Chen, Y. Tang, S. Wei, G. Niu, Tensile and indentation creep behavior of Mg-5% Sn and Mg-5% Sn-2% Di alloys, *Mater. Sci. Eng.: A* 464 (1) (2007) 124–128.
- [6] S.-h. Wei, Y.-g. Chen, Y.-b. Tang, M. Liu, S.-f. Xiao, X.-p. Zhang, Y.-h. Zhao, Compressive creep behavior of Mg-Sn binary alloy, *Trans. Nonferrous Met. Soc. China* 18 (2008) s214–s217.
- [7] X.-p. Zhang, Y.-g. Chen, S.-f. Xiao, Y.-b. Tang, G. Niu, S.-h. Wei, Y.-h. Zhao, Microstructure, tensile properties and compressive creep resistance of Mg-(5–8.5)% Sn-2%La alloys, *Trans. Nonferrous Met. Soc. China* 18 (2008) s299–s305.
- [8] M. Yang, F. Pan, Effects of Y addition on as-cast microstructure and mechanical properties of Mg-3Sn-2Ca (wt%) magnesium alloy, *Mater. Sci. Eng.: A* 525 (1) (2009) 112–120.
- [9] C. Zhao, X. Chen, F. Pan, S. Gao, D. Zhao, X. Liu, Effect of Sn content on strain hardening behavior of as-extruded Mg-Sn alloys, *Mater. Sci. Eng.: A* 713 (2018) 244–252.
- [10] S. Wei, Y. Chen, Y. Tang, X. Zhang, M. Liu, S. Xiao, Y. Zhao, Compressive creep behavior of Mg-Sn-La alloys, *Mater. Sci. Eng.: A* 508 (1) (2009) 59–63.
- [11] H. Liu, Y. Chen, H. Zhao, S. Wei, W. Gao, Effects of strontium on microstructure and mechanical properties of as-cast Mg-5wt%Sn alloy, *J. Alloy. Comp.* 504 (2) (2010) 345–350.
- [12] F. Pan, M. Yang, Preliminary investigations about effects of Zr, Sc and Ce additions on as-cast microstructure and mechanical properties of Mg-3Sn-1Mn (wt%) magnesium alloy, *Mater. Sci. Eng.: A* 528 (15) (2011) 4973–4981.
- [13] R.G. Guan, Y.F. Shen, Z.Y. Zhao, R.D.K. Misra, Nanoscale precipitates strengthened lanthanum-bearing Mg-3Sn-1Mn alloys through continuous rheo-rolling, *Sci. Rep.* 6 (2016) 23154.
- [14] C.Q. Liu, H.W. Chen, H. Liu, X.J. Zhao, J.F. Nie, Metastable precipitate phases in Mg-9.8 wt%Sn alloy, *Acta Mater.* 144 (2018) 590–600.
- [15] J. Gao, Ya Chen, Y. Wang, Effect of Sn element on the formation of LPSO phase and mechanical properties of Mg-6Y-2Zn alloy, *Mater. Sci. Eng.: A* 711 (2018) 334–342.
- [16] S. Zhu, T. Luo, Y. Yang, Improving mechanical properties of age-hardenable Mg-6Zn-4Al-1Sn alloy processed by double-aging treatment, *J. Mater. Sci. Technol.* 33 (11) (2017) 1249–1254.
- [17] G. Nayyeri, R. Mahmudi, F. Salehi, The microstructure, creep resistance, and high-temperature mechanical properties of Mg-5Sn alloy with Ca and Sb additions, and aging treatment, *Mater. Sci. Eng.: A* 527 (21) (2010) 5353–5359.
- [18] F.R. Elsayed, T.T. Sasaki, C.L. Mendis, T. Ohkubo, K. Hono, Compositional optimization of Mg-Sn-Al alloys for higher age hardening response, *Mater. Sci. Eng.: A* 566 (2013) 22–29.
- [19] T.T. Sasaki, F.R. Elsayed, T. Nakata, T. Ohkubo, S. Kamado, K. Hono, Strong and ductile heat-treatable Mg-Sn-Zn-Al wrought alloys, *Acta Mater.* 99 (2015) 176–186.
- [20] S. Wei, Y. Chen, Y. Tang, H. Liu, S. Xiao, G. Niu, X. Zhang, Y. Zhao, Compressive creep behavior of as-cast and aging-treated Mg-5wt% Sn alloys, *Mater. Sci. Eng.: A* 492 (1) (2008) 20–23.
- [21] Y.K. Kim, S.W. Sohn, D.H. Kim, W.T. Kim, D.H. Kim, Role of icosahedral phase in enhancing the strength of Mg-Sn-Zn-Al alloy, *J. Alloy. Comp.* 549 (2013) 46–50.
- [22] X. Huang, Y. Du, W. Li, Y. Chai, W. Huang, Effects of Ag content on the solid-solution and age-hardening behavior of a Mg-5Sn alloy, *J. Alloy. Comp.* 696 (2017) 850–855.
- [23] H.-s. Xue, Z.-h. Xing, W.-n. Zhang, G. Yang, F.-s. Pan, Effects of ultrasonic treatment on microstructure and mechanical properties of Mg-6Zn-0.5Y-2Sn alloy, *Trans. Nonferrous Met. Soc. China* 26 (7) (2016) 1826–1834.
- [24] T. Hu, W. Xiao, F. Wang, Y. Li, S. Lyu, R. Zheng, C. Ma, Improving tensile properties of Mg-Sn-Zn magnesium alloy sheets using pre-tension and ageing treatment, *J. Alloy. Comp.* 735 (2018) 1494–1504.
- [25] R.G. Guan, Z.Y. Zhao, H. Zhang, C. Lian, C.S. Lee, C.M. Liu, Microstructure evolution and properties of Mg-3Sn-1Mn (wt%) alloy strip processed by semisolid rheo-rolling, *J. Mater. Process. Technol.* 212 (6) (2012) 1430–1436.
- [26] F. Zhang, S. Liu, Y. Du, Experimental investigation and thermodynamic modeling of the La-Mg system, *J. Alloy. Comp.* 663 (2016) 279–288.
- [27] C. Guo, Z. Du, Thermodynamic assessment of the La-Mg system, *J. Alloy. Comp.* 385 (1) (2004) 109–113.
- [28] T. Link, A. Epishin, U. Brückner, P. Portella, Increase of misfit during creep of superalloys and its correlation with deformation, *Acta Mater.* 48 (8) (2000) 1981–1994.
- [29] M. Zhang, W.-z. Zhang, G.-z. Zhu, K. Yu, Crystallography of Mg_2Sn precipitates in Mg-Sn-Mn-Si alloy, *Trans. Nonferrous Met. Soc. China* 17 (6) (2007) 1428–1432.
- [30] X.F. Huang, W.Z. Zhang, Improved age-hardening behavior of Mg-Sn-Mn alloy by addition of Ag and Zn, *Mater. Sci. Eng.: A* 552 (2012) 211–221.
- [31] G. Zhang, J. Chen, H. Yan, B. Su, X. He, M. Ran, Effects of artificial aging on microstructure and mechanical properties of the Mg-4.5Zn-4.5Sn-2Al alloy, *J. Alloy.*

- Comp. 592 (2014) 250–257.
- [32] B. Song, T. Wang, H. Sun, et al., Two-step hydrothermally synthesized carbon nanodots/WO₃ photocatalysts with enhanced photocatalytic performance, *Dalton Trans.* 46 (2017) 15769–15777.
- [33] C. Lin, H. Hu, C. Cheng, et al., Nano-TiNb₂O₇/carbon nanotubes composite anode for enhanced lithium-ion storage, *Electrochim. Acta* 260 (2018) 65–72.
- [34] Y. Li, T. Jing, G. Xu, J. Tian, M. Dong, Q. Shao, B. Wang, Z. Wang, Y. Zheng, C. Yang, Z. Guo, 3-D magnetic graphene oxide-magnetite poly(vinyl alcohol) nanocomposite substrates for immobilizing enzyme, *Polymer* 149 (2018) 13–22.
- [35] X. Cui, G. Zhu, Y. Pan, et al., Polydimethylsiloxane-titania nanocomposite coating: fabrication and corrosion resistance, *Polymer* 138 (2018) 203–210.
- [36] C. Wang, B. Mo, Z. He, et al., Hydroxide ions transportation in polynorbornene anion exchange membrane, *Polymer* 138 (2018) 363–368.
- [37] C. Cheng, et al., Tunable and weakly negative permittivity in carbon/silicon nitride composites with different carbonizing temperatures, *Carbon* 125 (2017) 103–112.
- [38] Z. Wu, S. Gao, L. Chen, et al., Electrically insulated epoxy nanocomposites reinforced with synergistic core-shell SiO₂@MWCNTs and montmorillonite bifillers, *Macromol. Chem. Phys.* 218 (2017) 1700357.
- [39] W. Yang, X. Wang, J. Li, et al., Polyoxymethylene/ethylene butylacrylate copolymer/ethylene-methyl acrylate-glycidyl methacrylate ternary blends, in press, *Polym. Eng. Sci.* 58 (2018) 1127–1134.
- [40] H. Gu, H. Zhang, J. Lin, et al., Large negative giant magnetoresistance at room temperature and electrical transport in cobalt ferrite-polyaniline nanocomposites, *Polymer* 143 (2018) 324–330.
- [41] C. Wang, B. Mo, Z. He, et al., Crosslinked norbornene copolymer anion exchange membrane for fuel cells, *J. Membr. Sci.* 556 (2018) 118–125.
- [42] Y. Zhang, M. Zhao, J. Zhang, Q. Shao, J. Li, H. Li, B. Lin, M. Yu, S. Chen, Z. Guo, Excellent corrosion protection performance of epoxy composite coatings filled with silane functionalized silicon nitride, *J. Polym. Res.* 25 (2018) 130.
- [43] Y. Kong, Y. Li, G. Hu, et al., Preparation of polystyrene-b-poly(ethylene/propylene)-b-polystyrene grafted glycidyl methacrylate and its compatibility with recycled polypropylene/recycled high impact polystyrene blends, *Polymer* 145 (2018) 232–241.
- [44] Y. Wang, P. Zhou, S. Luo, et al., Controllable synthesis of monolayer poly(acrylic acid) on channel surface of mesoporous alumina for Pb(II) adsorption, *Langmuir* 34 (2018) 7859–7868.
- [45] K. Gong, Q. Hu1, L. Yao, M. Li, D. Sun, Q. Shao, B. Qiu, Z. Guo, Ultrasonic pre-treated sludge derived stable magnetic active carbon for Cr(VI) removal from wastewater, *ACS Sustain. Chem. Eng.* 6 (2018) 7283–7291.
- [46] J. Huang, Y. Cao, Q. Shao, X. Peng, Z. Guo, Magnetic nanocarbon adsorbents with enhanced hexavalent chromium removal: morphology dependence of fibrillar vs particulate structures, *Ind. Eng. Chem. Res.* 56 (2017) 10689–10701.
- [47] Z. Hu, D. Zhang, F. Lu, et al., Multistimuli-responsive intrinsic self-healing epoxy resin constructed by host–guest interactions, *Macromolecules* 51 (2018) 5294–5303, <https://doi.org/10.1021/acs.macromol.8b01124>.
- [48] K. Gong, Q. Hu, Y. Xiao, X. Cheng, H. Liu, N. Wang, B. Qiu, Z. Guo, Triple layered core-shell ZVI@carbon@polyaniline composites enhanced electron utilization in Cr(VI) reduction, *J. Mater. Chem. A* 6 (2018) 11119–11128.
- [49] J. Huang, Y. Li, Y. Cao, F. Peng, Y. Cao, Q. Shao, H. Liu, Z. Guo, Hexavalent chromium removal over magnetic carbon nanoadsorbent: synergistic effect of fluorine and nitrogen co-doping, *J. Mater. Chem. A* 6 (2018) 13062–13074.
- [50] Z. Hu, Q. Shao, Y. Huang, et al., Light triggered interfacial damage self-healing of poly(p-phenylene benzobisoxazole) fiber composites, *Nanotechnology* 29 (2018) 185602.
- [51] K. Sun, R. Fan, X. Zhang, Z. Zhang, Z. Shi, N. Wang, P. Xie, Z. Wang, G. Fan, H. Liu, C. Liu, T. Li, C. Yan, Z. Guo, An overview of metamaterials and their achievements in wireless power transfer, *J. Mater. Chem. C* 6 (2018) 2925–2943.
- [52] Y. Guo, G. Xu, X. Yang, K. Ruan, T. Ma, Q. Zhang, J. Gu, Y. Wu, H. Liu, Z. Guo, Significantly enhanced and precisely modeled thermal conductivity in polyimide nanocomposites by chemically modified graphene via in-situ polymerization and electrospinning-hot press technology, *J. Mater. Chem. C* 6 (2018) 3004–3015.
- [53] J. Gu, Y. Li, C. Liang, Y. Tang, L. Tang, Y. Zhang, J. Kong, H. Liu, Z. Guo, Synchronously improved dielectric and mechanical properties of wave-transparent laminated composites combining with outstanding thermal stability by incorporating isozyme/POSS functionalized PBO fibers, *J. Mater. Chem. C* 6 (2018) 7652–7660.
- [54] C. Wang, Z. He, X. Xie, et al., Controllable cross-linking anion exchange membranes with excellent mechanical and thermal properties, *Macromol. Mater. Eng.* 3 (2018) 1700462.
- [55] J. Lin, X. Chen, C. Chen, et al., Durably antibacterial and bacterially anti-adhesive cotton fabrics coated by cationic fluorinated polymers, *ACS Appl. Mater. Interfaces* 10 (2018) 6124–6136.
- [56] W. Deng, T. Kang, H. Liu, et al., Potassium hydroxide activated and nitrogen doped graphene with enhanced supercapacitive behavior, *Sci. Adv. Mater.* 10 (2018) 937–949.
- [57] H. Du, Y. An, Y. Wei, et al., Nickel powders modified nanocoating strengthened iron plates by surface mechanical attrition alloy and heat treatment, *Sci. Adv. Mater.* 10 (2018) 1063–1072.
- [58] Z. Hu, C. Wang, F. Zhao, et al., Fabrication of a graphene/C60 nanohybrid via gamma-cyclodextrin host-guest chemistry for photodynamic and photothermal therapy, *Nanoscale* 9 (2017) 8825.
- [59] Z. Hu, D. Zhang, L. Yu, Y. Huang, Light-triggered C60 release from a graphene/cyclodextrin nanoplatfor for the protection of cytotoxicity induced by nitric oxide, *J. Mater. Chem. B* 6 (2018) 518–526.